ADVANCED MATERIALS TECHNOLOGIES
www.advmattechnol.de

Microneedles for Enhanced Bacterial Pathogen Inactivation and Accelerated Wound Healing

*Akshay Krishnakumar, Nicholas L.F. Gallina, Devendra Sarnaik, Robyn R McCain, Christa Crain, Mason Tipton, Mohamed Seleem, Arun K. Bhunia, and Rahim Rahimi**

Bacterial wound infections are a significant socioeconomic concern in the modern healthcare industry owing to increased morbidity, prolonged hospital stay, and mortality. Bacterial infectious agents that colonize the wound bed develop biofilms, acting as a physical barrier that prevents the effective penetration of topical antimicrobials. Further, bacteria in such infectious wounds express a wide range of virulence factors promoting intercellular transmigration and host cell invasion complicating the treatment regimen. To address this need, a water-dissolvable poly-vinyl pyrrolidine (PVP), calcium peroxide (CPO) infused microneedle structure (denoted as PVP/CPO MN) for effective transdermal delivery of antimicrobial payload deep into the tissues is developed. Fluid exudate from the wound bed dissolves the PVP/CPO MN enabling the release of CPO deep into the infected wound bed. A slow catalytic decomposition of CPO results in the sustained release of reactive oxygen species (ROS) deep within the infected wound inhibiting the inter- and intracellular pathogens. Here, a systematic study of microneedle fabrication and sterilization after complete packaging is conducted to ensure scalability and safe applicability while maintaining mechanical and antibacterial properties. In vitro, antibacterial efficacy of the microneedles is validated against two common wound pathogens, *Pseudomonas aeruginosa (P. aeruginosa)* and *Staphylococcus aureus (S. aureus)*. Moreover, the PVP/CPO MN exhibited significant efficacy in eradicating both extracellular and intracellular bacterial populations within an in vivo porcine wound model. Additionally, the microneedle technology facilitated a faster wound healing, with ≈30% increase compared to control and a 15% improvement over conventional silver dressing.

1. Introduction

Chronically infected non-healing wounds (CNHWs) pose a significant and escalating burden on healthcare systems worldwide.[1] Among these, a staggering 10.5 million Medicare beneficiaries are affected in the United States alone, with the annual cost of managing such wounds exceeding $96.8 billion USD.[2,3] This number is projected to rise further due to the aging population and increasing prevalence of chronic diseases such as diabetes and obesity.[4] The physiological processes underlying CNHWs render them susceptible to infection, further exacerbating the challenges in wound management.[5] The compromised immune response and structural abnormalities in the tissue create an environment conducive to bacterial proliferation and colonization.[6] CNHWs are frequently colonized by a variety of bacteria, with *Staphylococcus aureus* (*S. aureus*) and *Pseudomonas aeruginosa* (*P. aeruginosa*) bacterium being particularly prevalent.[7] Studies have shown that up to 60% of CNHWs are infected with these bacteria, or often in combination with other pathogens.

A. Krishnakumar, R. Rahimi
School of Electrical and Computer Engineering
Purdue University
West Lafayette, IN 47907, USA
E-mail: rrahimi@purdue.edu
A. Krishnakumar, D. Sarnaik, R. Rahimi
Birck Nanotechnology Center
Purdue University
West Lafayette, IN 47907, USA
N. L. Gallina, A. K. Bhunia
Department of Food Science
Purdue University
West Lafayette, IN 47907, USA
N. L. Gallina
Purdue Institute of Inflammation
Immunology, and Infectious Disease
Purdue University
West Lafayette, IN 47907, USA
D. Sarnaik, R. Rahimi
School of Materials Engineering
Purdue University
West Lafayette, IN 47907, USA
R. R McCain, C. Crain, M. Tipton, A. K. Bhunia
Center for Comparative Translational Research
Purdue University
West Lafayette, IN 47907, USA
The ORCID identification number(s) for the author(s) of this article can be found under https://doi.org/10.1002/admt.202400219

DOI: 10.1002/admt.202400219

These bacteria have a distinct advantage in chronic wounds as they readily adhere to wound surfaces and secrete a slimy substance called a biofilm.[8,9] This biofilm acts as a protective shield, hindering the penetration of immune cells and topical antibiotics, making them extremely difficult to eradicate.[10]

Standard-of-care procedures for CNHWs often involve debridement to remove biofilm layers and necrotic tissue, followed by topical antibiotic therapy.[11] However, clinical studies have demonstrated limited effectiveness of these approaches, highlighting the need for alternative treatment modalities. Recent investigations have unveiled the role of virulence factors in facilitating invasion and dissemination within host tissues in the form of intercellular transmigration and intracellular invasion complicating the treatment regimen.[12–14] Intercellular transmigration allows bacteria to infiltrate and reside within the spaces between host cells, contributing to chronic infections observed in skin surfaces and deeper tissues.[15]

Furthermore, some bacteria can intracellularly invade and reside within host cells which allows them to replicate within the cell, evade immune surveillance, and manipulate host cell functions to their advantage.[16] Host cell invasion allows bacteria to establish persistent infections, resist antibiotic treatment, and cause tissue damage.[17] Such a phenomenon explains the difficulty in achieving complete inactivation of the bacterial infection with topical treatments and is linked to chronic infections observed in various epithelial linings, including the skin, lungs, and intestinal tract (e.g., cystic fibrosis, chronic rhinosinusitis, inflammatory bowel disease).[18–23] Intercellular and intracellular bacterial pathogenesis pose a significant challenge as they are difficult to reach with topical medications. In response to these challenges, various topical delivery technologies, such as ultrasonic-assisted and electrophoresis-based wound therapy methods, have been explored to enhance drug penetration into infected tissues. However, these techniques often require the use of bulky equipment and need for trained personnel, limiting their clinical utility.[24,25]

Recently microneedle (MN) technologies have emerged as a promising strategy for delivering therapeutics deep into tissue layers, bypassing biofilm barriers, and targeting intercellular pathogens effectively.[26–28] These micron-scale needles, fabricated from biocompatible polymers, offer a minimally invasive and versatile platform for drug delivery. Soluble MN incorporating degradable polymer composites has garnered significant attention for treating infected wounds with biofilm barriers.[29,30] These MN dissolve upon insertion into the wound, releasing the encapsulated therapeutic agent directly into the targeted tissue layer, bypassing the biofilm barrier and potentially reaching intercellular bacteria.[31] Over the past few years, numerous studies have investigated the use of MN loaded with various biocompatible and degradable polymers (e.g., Polyvinylpyrrolidone (PVP), Gelatin Methacrylate) in combination with different therapeutic agents.[32,33] These studies have shown promising results in treating infected wounds with biofilm layers. For example, a study by Ziesmer et al.[34] demonstrated the effectiveness of MN loaded with vancomycin against *MRSA* biofilms in a rat model. Such MN arrays provide an effective treatment to eliminate *MRSA*-associated skin and soft tissue infections (SSTIs) while reducing the emergence of VAN-resistant *MRSA* strains in uninfected body parts. Another study by Abdelghany et al.[35] showed that MN containing ciprofloxacin could effectively treat *S. aureus* infections on different in vitro and ex vivo wound models. Recent advancements in MN-based wound therapy systems have also explored combined therapies using antibiotics alongside growth-promoting agents to enhance wound healing.[36]

However, a major concern with antibiotic-based therapies is the rapid emergence of antibiotic-resistant bacterial strains.[37–39] The constant exposure to antibiotics can induce changes in the phenotype and genotype of the bacteria, leading to reduced susceptibility to antibiotics which can consequently reduce MN efficacy. In addition, while reported MN effectively bypasses the biofilm and reaches intercellular bacteria, it currently lacks the capability to target intracellular bacteria. The limited diffusion of antibiotics within host cells hampers their ability to penetrate and eradicate these deeply entrenched pathogens.[40] This highlights the need for alternative compounds that can target intracellular and intercellular bacterial colonies. Researchers have explored the potential of antibacterial agents such as silver ions and reactive oxygen species (ROS) for more effective eradication within intercellular and intracellular regions.[41,42] While silver ions have shown promising antibacterial properties and have been incorporated into microneedle technologies, they face a significant drawback of high toxicity. Silver ions can induce further inflammation in the host tissue, potentially delaying wound healing process.[41] In contrast, reactive oxygen species (ROS) at specific concentrations exhibit unique bactericidal characteristics without harming native cells.[43,44] Studies have shown that slow-releasing ROS compounds, such as calcium peroxide (CPO), effectively eradicate various bacterial strains with minimal resistance development through catalytic degradation upon exposure to biofluids.[45,46] Integrating these compounds in the form of nanoparticles or microparticles within dissolving microneedles offers a compelling strategy for CNHW treatment. These microneedles can bypass the biofilm layer, deliver the payload deep into the tissue, and target both intercellular and intracellular bacteria.

To address this need here we have investigated the utilization of a flexible microneedle array composed of PVP as the water-soluble polymer that contains calcium peroxide as the active ingredient for delivery into the skin tissue. Upon application, the MN dissolves and releases the CPO particles deep into the infected wound bed. Upon exposure to water, CPO produces hydrogen peroxide (H_2O_2) at a slow rate, facilitating the prolonged release of reactive oxygen species (ROS) to the wound bed (**Figure 1**).[47] Moreover, the slow production of ROS from CPO decomposition can selectively target pathogen-infected weaker host cells (Figure S1 (Supporting Information) provided in

M. Seleem
Department of Biomedical Sciences and Pathobiology
Virginia Polytechnic Institute and State University
Blacksburg, VA 24061, USA
A. K. Bhunia
Department of Comparative Pathobiology
Purdue University
West Lafayette, IN 47907, USA

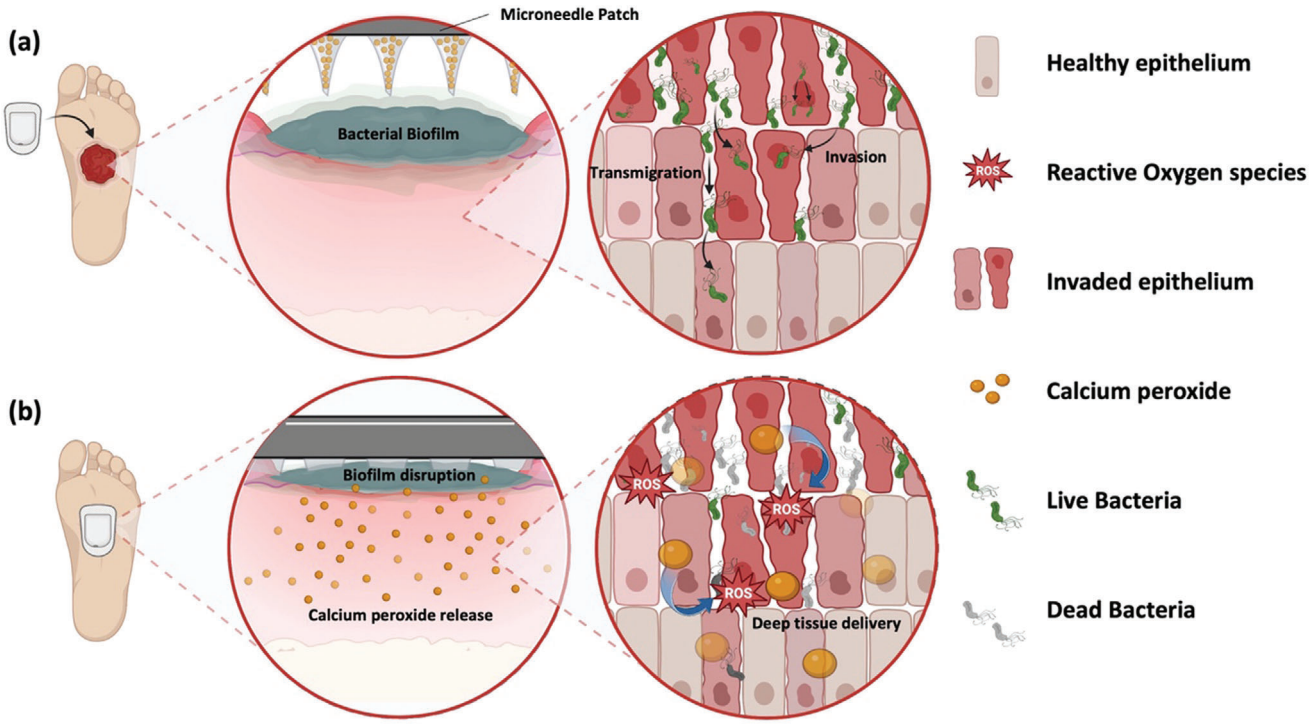

Figure 1. The impact of microneedle treatment on wounds with biofilm infection. a) Progression of a bacterial infection on a wound before microneedle placement, showing biofilm formation, as well as intercellular and intracellular pathogenesis of the bacteria. b) Mechanism of action of microneedles applied to the wound, bypassing the biofilm physical barrier with rapid dissolution and release of calcium peroxide (CPO) into the tissue, creating reactive oxygen species to eradicate the infection and stimulate tissue regeneration.

Supporting Information). Such selectivity is achieved as most of the predominant infectious bacterial pathogens[48] that colonize the wound bed, produce exotoxins such as cytolysins,[49] alpha toxins,[50] cytotoxin, and endotoxin[51] that severely weaken the host cell membrane. Additionally, these pathogens also scavenge iron from host sources thereby compromising the superoxide dismutase responsible for developing the natural ROS tolerance of the host.[52] While previous studies including efforts from our lab have investigated the use of calcium peroxide in nanofibers or microneedles for treating topical skin infections, they have primarily focused on the bactericidal properties.[45] These studies haven't fully explored the potential for eradicating both intercellular and intracellular pathogens and their impact on wound healing. Additionally, most research has focused on proof-of-concept, neglecting the crucial aspects of scalability and practical implementation for clinical use. Furthermore, for any technology to be of practical use it needs to undergo standard packaging and sterilization processes without compromising its functionality. As such, one of the main focuses of this work was to investigate the scalable and rapid production of these MNs, along with an effective sterilization procedure that does not compromise the MNs' functionality. Through a combination of systematic in vitro and in vivo studies, we validated the effectiveness of the MN in eradicating intercellular and intracellular infections and accelerating wound healing, laying the groundwork for their clinical translation and widespread adoption in wound care practice.

2. Experimental Section

2.1. Microneedle Fabrication and Mechanical Testing

The proposed strategy utilizes a simple two-step transfer method for developing MN structures using stereolithography (Form 3 by Formlabs Inc., Somerville, MA, USA). In this technique, MN master patterns were developed on a circular substrate with a diameter of 20 mm with the needle height and base as 1.7 and 0.75 mm, respectively. The 3D-printed MN master pattern was immersed in Isopropyl Alcohol (IPA) and subjected to gentle shaking followed by a final post-UV curing step for 10 min at 60 °C.[53] After drying, the 3D-printed structures were spray-coated with a layer of boron nitride (BN) dry film lubricant (Dupont, Wilmington, DE, USA) and dried at 100 °C for 10 min in a conventional oven. Next, the MN was affixed to a weighing boat using double-sided tape, and a prepolymer solution of polydimethylsiloxane (PDMS) mixture (Dow, Auburn, MI, USA) with a 10:1 ratio of base to curing agent was poured on top of the master pattern. The weighing boats were placed in a vacuum chamber at 1 kPa for 20 min to remove any bubbles from the PDMS solution followed by curing in the oven at 70 °C for 5 h. The cured negative PDMS mold was then carefully removed from the 3D printed MN structure, followed by spray coating of BN as described before, facilitating the easy release of the structure from the mold. Progressively, a premixed solution of *N*-Vinyl Pyrrolidine (NVP, Sigma-Aldrich, St. Louis, MO, USA) containing

1 wt% photoinitiator (651 Ciba Specialty Chemicals, Switzerland) and 10 wt% of CPO was pipetted into the PDMS negative mold. Additionally, a commercially available fabric cloth (TechniCloth II, Glenview, IL, USA) was added as a backing layer for the MN structures, followed by UV irradiation for 30 min to completely cure and polymerize the NVP monomer containing CPO. The fully cured CPO-infused PVP MN structures (PVP/CPO) along with the PDMS mold were subsequently packaged in a standard dry heat sterilization pouch (PlastCare USA, Chatsworth, CA, USA) and were heat sterilized using the Sterident 300 Dry Heat Sterilizer (West Nyack, NY, USA). The MN structures were then heat sterilized using the standard dry heat sterilization temperatures for sterilizing medical equipment: 150 °C for 150 min, 160 °C for 120 min, 170 °C for 60 min, and 180 °C for 30 min. The heat-treated MN structures were stored at room temperature conditions and were removed from the sterilization bag and PDMS mold at the experiment time points (**Figure 2a**). Next, the effective polymerization and crosslinking between the NVP monomer and presence of CPO within the polymeric matrix was validated using Attenuated Total Reflection Fourier Transform Infrared Spectroscopy (ATR-FTIR) with an Id7 ATR accessory attached to a Nicolet iS 5 FTIR Spectrometer (ThermoFisher, MA, USA).

To investigate the effect of heat-sterilization temperatures on the mechanical integrity of the MNs, fracture tests were performed under an axial compression load using a displacement-force station (Universal testing machine, ADMET eXpert 400, MTEST Quattro). For this test, the heat-treated MNs were detached from the PDMS mold and affixed to the moving side of the instrument using double-sided tape. An axial force was then applied toward the flat aluminum surface, oriented perpendicularly to the axis of the moving mount, at a speed of 1.1 mm s^{-1} until a preset displacement of was reached. The force and displacement data were used to finally evaluate the fracture force and stiffness of the MN treated at different sterilization temperatures.

2.2. Antibacterial Analysis

2.2.1. Planktonic Studies

Initially, to validate the bactericidal efficacy of the CPO-infused MN patches, in vitro antibacterial test was conducted against a model Gram-positive (*Staphylococcus aureus* ATCC 25 923, *Enterococcus faecalis* ATCC 29212) and Gram-negative (*Pseudomonas aeruginosa* ATCC 25668, *Escherichia coli* K88 (F4)+) bacteria.[54] Initially, all four bacterial strains were revived from the frozen stock and cultured overnight in a sterile Brain Heart Infusion (BHI, 15 g L^{-1}, Sigma-Aldrich, St. Louis, MO, USA) at 37 °C. Next, the overnight culture was washed in PBS three times and diluted to an OD_{600nm} of 0.25 which corresponds to $\approx 10^8$ CFU mL^{-1}. To assess the planktonic bactericidal property of the MN, 200 µL of diluted bacterial suspensions were added to a 96-well plate, followed by the application of PVP/CPO MN structures treated with different sterilization temperatures. After 6 h of incubation, the viable bacteria from the bacterial solutions were serially diluted in PBS and plated on BHI agar plates, and the colonies were counted after overnight incubation. All experiments were repeated three times and plated 6 times (providing 3 biological and 2 technical replicates of each well) for statistical analysis.

2.2.2. Biofilm Studies

Furthermore, to investigate the efficacy of the developed MN treatment against biofilm infection, a simple and effective biofilm wound model was developed.[55] Initially, 100 µL of the washed and normalized bacterial suspensions were uniformly spread onto a BHI agar plate and incubated at 37 °C for 24 h (1st day). Subsequently, 2 mL of fetal bovine serum (Gibco, ThermoFisher, Waltham, MA, USA) was spread across to the agar plate, followed by incubation at 37 °C for an additional 24 h (2nd day) which aids the development of a thick mature biofilm structure. Next, the PVP/CPO MN structures sterilized at different temperatures were applied onto the biofilm surface, followed by further incubation for another 24 h. Finally, the MN-treated surface was aseptically sampled using a sterile biopsy punch (ø = 6 mm, AcuPunch) and sonicated in 1 mL of PBS solution for 5 min. The solution was serially diluted and plated onto a BHI agar plate to evaluate the viable bacterial counts. Additionally, the MN treatment group treated at the optimal sterilization temperature was exposed to the biofilm model repeatedly for 5 days by replacing the patch every 24 h in order to determine the minimum number of days of treatment required to achieve complete eradication. As previously described, the treated biofilm surface was aseptically sampled every 24 h, followed by the reapplication of a fresh MN patch to the same location. The samples were further sonicated in PBS, serially diluted, and plated onto a BHI agar plate to extract the viable bacterial counts.

2.3. Biocompatibility and Pathogen Inactivation Analysis

2.3.1. Biocompatibility Studies

To validate the safety and efficacy of the MN treatment to the wound bed upon exposure and determine the potential toxicity of the materials or process, in vitro biocompatibility assessment was performed. For this test, human epithelial cells (HCT-8; CCL-244, ATCC, passage #10 and 12), cultured in Dulbecco's modified Eagle's medium (DMEM medium (Invitrogen Inc., Carlsbad, CA, USA) supplemented with 10% fetal bovine serum (Gibco, ThermoFisher, Waltham, MA, USA) and 1% Penicillin/Streptomycin (Waltham, ThermoFisher, MA, USA) was used. Initially, the frozen stocks were cultured in a T-75 flask at 37 °C in a humidified environment (95%) with 5% carbon dioxide for 3 days until 80% confluency. Sequentially, the cells were trypsinized, detached, washed, and diluted to a concentration of 5000 cells mL^{-1} for cell proliferation, live-dead, and trypan blue stain testing. Initially, the metabolic viability of the HCT-8 cells was assessed by calculating the % cell viability using a standard WST-8 assay (Abcam, Cambridge, UK).[56] To conduct this assay, 200 µL of the diluted cell suspensions were seeded into three separate 96-well plates and incubated for 24 h in the incubator to facilitate cell attachment, followed by the addition of the MN patches. After a day of MN exposure, the residual fabric was removed from all three

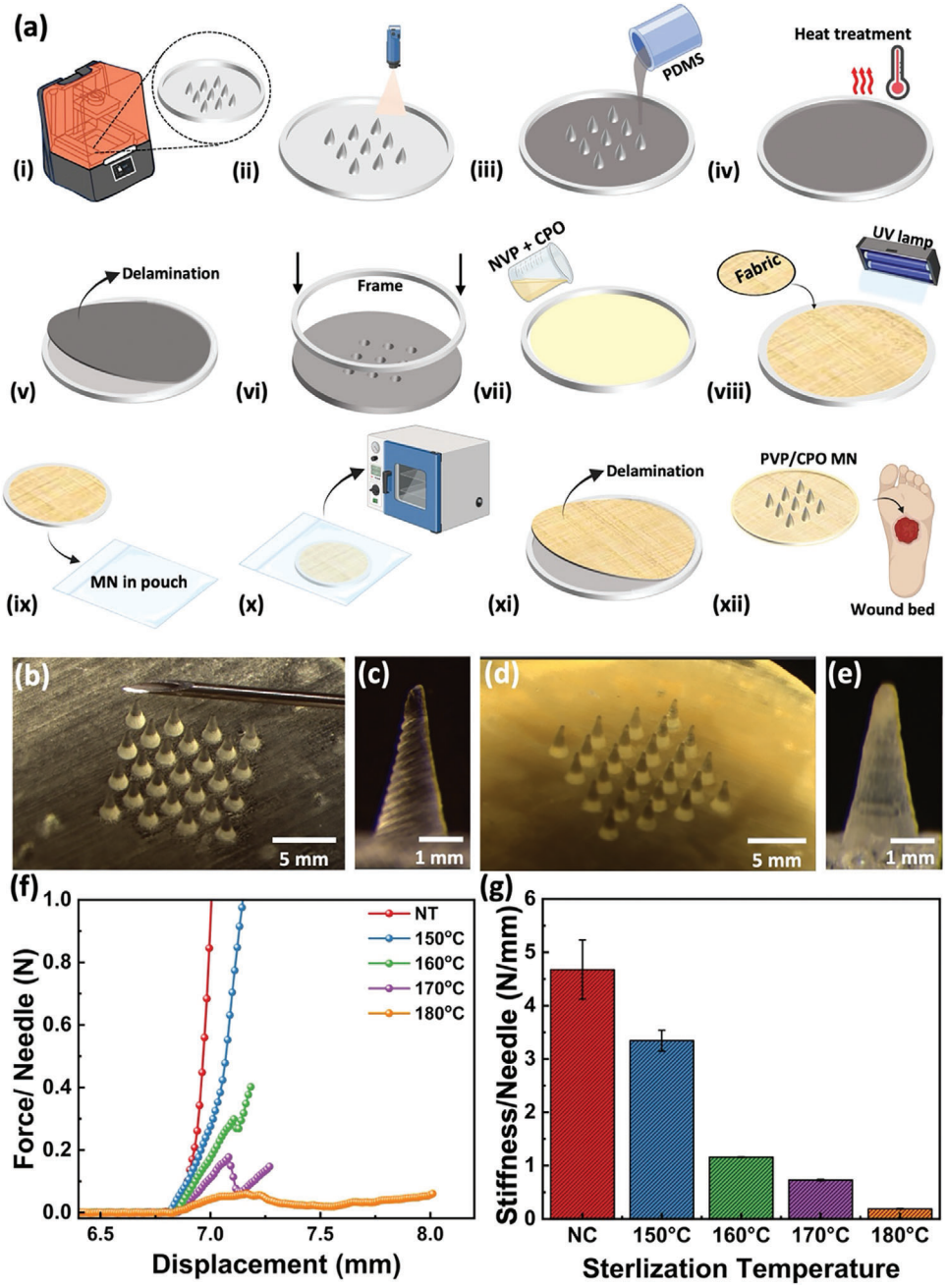

Figure 2. Fabrication and mechanical characterization. a) Schematic illustration of the MN development process: (i) 3D printing of MN, (ii) hydrophobic coating, (iii) casting of PDMS prepolymer solution, and (iv) curing the mold, (v) PDMS delamination, (vi) frame attachment, (vii) casting of PVP/CPO prepolymer solution, (viii) fabric attachment and UV curing, (ix) placement in autoclave pouch, (x) heat sterilization, (xi) removal of PVP/CPO MNs from PDMS support mold, and (xii) application to the wound site. b) Microscopic images of the 3D printed master mold MN array and c) high-magnification image of a single microneedle. d) Microscopic image of PVP/CPO MN array and e) high-magnification image of a single needle. f) Mechanical force versus displacement and g) mechanical stiffness characteristics of PVP/CPO MNs after sterilization at different temperatures. (NT refers to PVP/CPO MNs without heat sterilization treatment).

96-well plates, and a WST-8 proliferation assay was performed on the first 96-well plate. Meanwhile, the other two 96-well plates had fresh MN patches applied and were incubated for another 24 h. After the second 24 h, the second 96 well plate was tested for WST-8, while the third well plate had another MN patch added and was further incubated for an additional 24 h before conducting the test. The absorbance of resulting from the addition of the WST-8 reagents in the well plate was measured at 550 nm using a BMG Labtech clariostar (NC, USA) to evaluate the % cell viability.[57,58]

Next, to visualize the cell viability after MN exposure, two complimentary staining methods were used namely: LIVE/DEAD

Viability/Cytotoxicity Kit (ThermoFisher, Massachusetts, USA) and Trypan blue staining (Waltham, ThermoFisher, MA, USA). The Trypan blue staining provides a quick and simple method to estimate overall cell viability, while live-dead staining imaging offers more detailed information about cell membrane integrity and functions. The cells were diluted and seeded into a 12-well plate according to the previously described protocol, followed by exposure to MN treatment for 3 days with replacement every day. For the trypan blue staining process, MN patches were removed from the wells followed by the addition of 1 mL of 0.4% dye in PBS solution and incubated for 3 min at room temperature. On the other hand, for the live-dead fluorescent staining, the green (calcein) and red (ethidium homodimer) fluorescent dyes were incubated with the cells for 45 min, followed by cell imaging under an inverted microscope.[59,60] Cell imaging was performed after days 1 and 3 using a Nikon Ti2 Eclipse microscope (NY, USA), equipped with their respective filters, under a 10x and 40x optical lens. The obtained images were analyzed using NIS-Elements D software.

2.3.2. Pathogen Inactivation

Next, an in vitro infection model was developed using human epithelial Caco-2 cells (HTB-37, ATCC, passage # 23 and 30) to evaluate the antimicrobial activity of the MN patch against bacterial pathogenesis such as adhesion, intracellular invasion, and intercellular translocation.[61] Briefly, Caco-2 cells were seeded into two 12-well cell culture plates and trans well plates (Corning, 24-mm, 3-µm pore size) at a density of 5000 cells mL^{-1}, followed by incubation for 7 days. Upon reaching cell confluency, 100 µL (8-log CFU) of bacterial cultures (multiplicity-of-infection of 100) were added to the well plates containing the Caco-2 monolayer to mimic a bacterially infected in vitro wound model for 1 h. Next, MN patches were applied to the bacterially infected cell layer followed by further incubation for 1 h at 37 °C. For the adhesion assay, MN treatments were removed from the 12-well plate, followed by PBS washing and treatment with 500 µL of 0.5% sodium dodecyl sulfate per well for 5 min, followed by vigorous aspiration. The obtained solutions were vortexed, serially diluted, and plated on selective agar plates for bacterial adhesion counts. For the intracellular invasion assay, the patches were removed from the 12-well plate and washed with PBS, followed by treatment with DMEM without FBS containing 500 µL of gentamicin (50 µg mL^{-1}, Sigma Aldrich, St. Louis, MO, USA) for 1 h. The gentamicin antibiotic incubation aids in the inactivation of adherent and intercellularly transmigrated bacterial pathogens, thereby selectively evaluating the invaded pathogens. Next, the cell monolayers were further washed with PBS and lysed with 1% Triton X-100 (Sigma Aldrich, St. Louis, MO, USA) and plated on selective media for the CFU counts. The exact adhesion bacterial counts were calculated by subtracting the total number of CFU obtained from the invasion data. Additionally, for intercellular translocation analysis, the top insert chamber of the transwell was removed, followed by serial dilution and plating of the media solution from the basolateral (lower chamber) to extract the intercellularly migrated bacterial count. All bacterial counts from adhesion, invasion, and translocation assays were calculated as a percentage reduction against control samples to evaluate the bactericidal efficiency of the MN treatment against the pathogens.

2.3.3. In Vivo Wound Efficacy Assessment

In order to evaluate the efficacy of the developed treatment in a physiologically relevant skin condition, an in vivo porcine excision wound model was utilized. All protocols for the in vivo assessment followed the Institutional Animal Care and Use Committee (IACUC) approved protocol at Purdue Translational Pharmacology facility, under the supervision of a staff veterinarian. For this test, six adolescent pigs (age 5–6 months) weighing ≈50 kg each were acquired from a local farm and acclimated to the surroundings for 2 weeks. Next, the pigs were then anesthetized using a nose cone with 0–5% isoflurane and 2 LPM O_2, followed by shaving and cleaning of their dorsal region with 2% chlorhexidine scrub and saline rinse. Twelve full-thickness round wounds (ø = 12 mm) were introduced on the dorsal side of the pigs using a biopsy punch followed by local treatment with Nocita (liposomal bupivacaine) every 24 h (for 3 days) to manage their wound pain. Additionally, the pigs also received daily injections of carprofen (NSID) for pain and inflammation management over a period of 5 days. After developing the wound bed, the pigs were randomly assigned to groups of three, with one group receiving *P. aeruginosa* and another receiving *S. aureus* bacterium. In this process, each wound bed was then added with 50 µL of a washed and OD-normalized bacterial suspension containing 8-log CFU of the respective bacteria. The wounds were covered with sterile gauze held in place with Tegaderm and allowed to stay for 24 h to aid in infection development. Next, the three wounds on each pig were assigned to one of four treatment groups: control (sterile gauze), Acticoat (standard of care silver dressing), PVP MN structures, and PVP/CPO MN structures. All treatments were applied to each pig for 24 h and replaced daily for five consecutive days, with wound examination continuing for 14 days or until the euthanasia of the animals. On treatment days, a quantitative superficial swab was collected from the wound surface to assess infection levels, progression, and therapeutic responses throughout the treatment week. Each day until the end of treatment, a sterile cotton swab was used to collect a representative microbiological sample directly from the wound area after removing residuals from the previous day's treatment. The collected swabs, suspended in 1 mL of PBS were sonicated for 25 min followed by vortexing, serial dilution, and plating on selective media to obtain CFU/wound bacterial counts. Additionally, representative images of the wound beds were collected every day throughout the experimentation timeline to analyze the wound healing rate in all treatment groups for both bacterial infections. Finally, by day 14^{th}, the pigs were transported to the surgical scape and a fatal injection of Ethanol-D (390 mg mL^{-1}) at 1 mL per 10 lb body weight was administered using a cardiac stick to euthanize the pigs. After euthanasia, the reduction in intracellular invasion characteristics of the bacterium in response to the treatment was analyzed by resecting the section of the wound bed. The recovered wound tissues were then transported in a sterile conical tube and incubated in 50 µg mL^{-1} of gentamicin in 3 mL of DMEM for 2 h. Subsequently, the cells were washed three times in sterile PBS media, and the tissues were macerated with a tissue grinder. The

resulting suspension was further sonicated for 15 min, serially diluted, and plated to estimate the intracellular bacterial CFU/wound.

2.3.4. Statistical Analysis

All data collected for antimicrobial and biocompatibility tests were subjected to a one-way ANOVA test ($\alpha = 0.05$) followed by Dunnet's Test for multiple comparisons to validate statistical relevance and differences between conditions.

3. Results and Discussion

3.1. Microneedle Fabrication and Mechanical Testing

The developed 3D printed MN master mold, along with a single needle high magnification image is shown in Figure 2b,c. The MNs were designed with a height of 1.7 mm for the master mold and a base thickness of 0.75 mm, ensuring a specific aspect ratio for optimal functionality. At higher magnification in Figure 2c, minor ripples (≈20 µm) are observed along the MN structure, angled at 45° along the master mold, attributable to the resolution and the angular printing orientation of 3D printing. The final master mold observed an average height of ≈1.69 ± 0.03 mm per needle with a base thickness of 0.75 mm. Conversely, the final transferred PVP/CPO MN structure exhibited a relatively smooth surface while preserving the aspect ratio of the original master mold with a height of ≈1.65 ± 0.04 mm and an average thickness of ≈0.72 ± 0.06 mm (Figure 2d). The observation could be attributed to the BN coating that enhances the surface smoothness while also aiding the ease of MN detachment from the PDMS surface. Also, the yellowish opaque appearance of the MN confirms the uniform distribution of CPO along the structure as observed in Figure 2e. The polymerization of the NVP monomer and the presence of the CPO inside the PVP/CPO composite matrix was confirmed from the FTIR analysis as shown in Figures S2,S3 (Supporting Information). The transferred PVP/CPO MN (≈1.65 mm) was reported to have a sufficient length to penetrate the biofilm and epidermal/dermal layer of the skin, consequently facilitating a painless way of delivering antimicrobials into the wound bed.[62] Next, the mechanical integrity of the MNs treated at various heat-sterilization temperatures was investigated by performing a force-displacement curve analysis. All mechanical tests were performed up to a force of 35 N (≈1.4 N per needle) which will provide sufficient stiffness and strength to penetrate the biofilm and skin.[63,64] As observed in Figure 2f, all MN structures displayed an initial increase in force relative to the displacement change when subjected to axial compression force against a flat aluminum surface. Upon further displacement, the MN reached a point of fracture, known as the fracture force. As observed, the unsterilized MN showed no fracture force until the preset force of 35 N (≈1.4 N per needle) elucidating its strong mechanical performance. On the other hand, the 150 °C heat-sterilized MN structures showed no fracture force, similar to that of the unsterilized MN, indicating negligible impact of sterilization on mechanical properties. However, MNs treated at higher sterilization temperatures exhibited noticeable reduction fractures at 0.3, 0.15, and 0.5 N per needle toward 160, 170, and 180 °C, respectively. Such reduction in the mechanical properties was attributed to the decomposition of CPO at high temperatures, leading to the formation of micro defects along the structures and compromising the MN's mechanical integrity. Consequently, the slope of the force-displacement test was calculated to evaluate the MN's ability to resist fracture in response to the applied force, termed stiffness. As observed from Figure 2 g, the unsterilized MN structures a maximum stiffness of ≈4.6 N mm^{-1} from the force–displacement curve.[65] In addition, the 150 °C heat-sterilized MN structures showed no significant reduction in the stiffness profile as compared to that of the unsterilized samples. However, the MN structures subjected to higher sterilization temperatures exhibited a sequential and drastic reduction in stiffness profile to ≈0.3 at 180 °C. These results clearly elucidate that the MN structures treated at 150 °C did not exhibit fracture force until reaching the preset force while maintaining comparable stiffness to that of the unsterilized samples.

3.2. In Vitro Antibacterial Assessment

Next, bactericidal efficacy of the PVP/CPO MN patches treated at different sterilization temperatures was tested against the planktonic bacterium (Figure S4 Supporting Information). All PVP MN patches showed a minimal antibacterial efficacy < ≈0.5-log CFU and ≈1-log CFU toward *P. aeruginosa* and *S. aureus* bacterial populations respectively. On the other hand, PVP/CPO MN showed complete inhibition (undetectable) of the bacterial population (8-log CFU reduction) irrespective of their sterilization temperatures (**Figure 3**b,c). Similarly, the MN structures tested against enterotoxigenic *E. coli* and another common opportunistic pathogen, *E. faecalis*, exhibited similar results, with complete inhibition (undetectable, 8-log CFU) observed after 6 h of treatment (Figure S4a, Supporting Information). These results clearly explain that no noticeable change in the planktonic bactericidal performance was observed by treating the MN at dry heat sterilization temperatures.

Next, the bactericidal efficacy of the MN structures was tested against an in vitro biofilm model (Figure 3d). Similar to the previous results, the PVP MN structures showed an approximate ≈1.1-log CFU reduction to that of the control samples toward *P. aeruginosa*. This slight inhibitory effect could be explained due to the physical barrier developed by PVP dissolution thereby restricting bacterial proliferation. On the other hand, PVP/CPO MN showed an average reduction of 4.6-log CFU reduction across different sterilization temperatures in a *P. aeruginosa* biofilm model (Figure 3e). Similarly, an average 3.8-log CFU reduction was observed for the PVP/CPO MN across all sterilization conditions in the *S. aureus* biofilm model as shown in Figure 3f. This observation was due to the natural production of catalase by the *S. aureus* bacterial population which slightly reduces the therapeutic effect of the MN treatment. Similar reductions in the bacterial populations were observed for the MN when tested against *E. coli* and *E. faecalis* bacterial populations in a biofilm model (Figure S4b Supporting Information). It is also evident from these results that the effect of sterilization did not

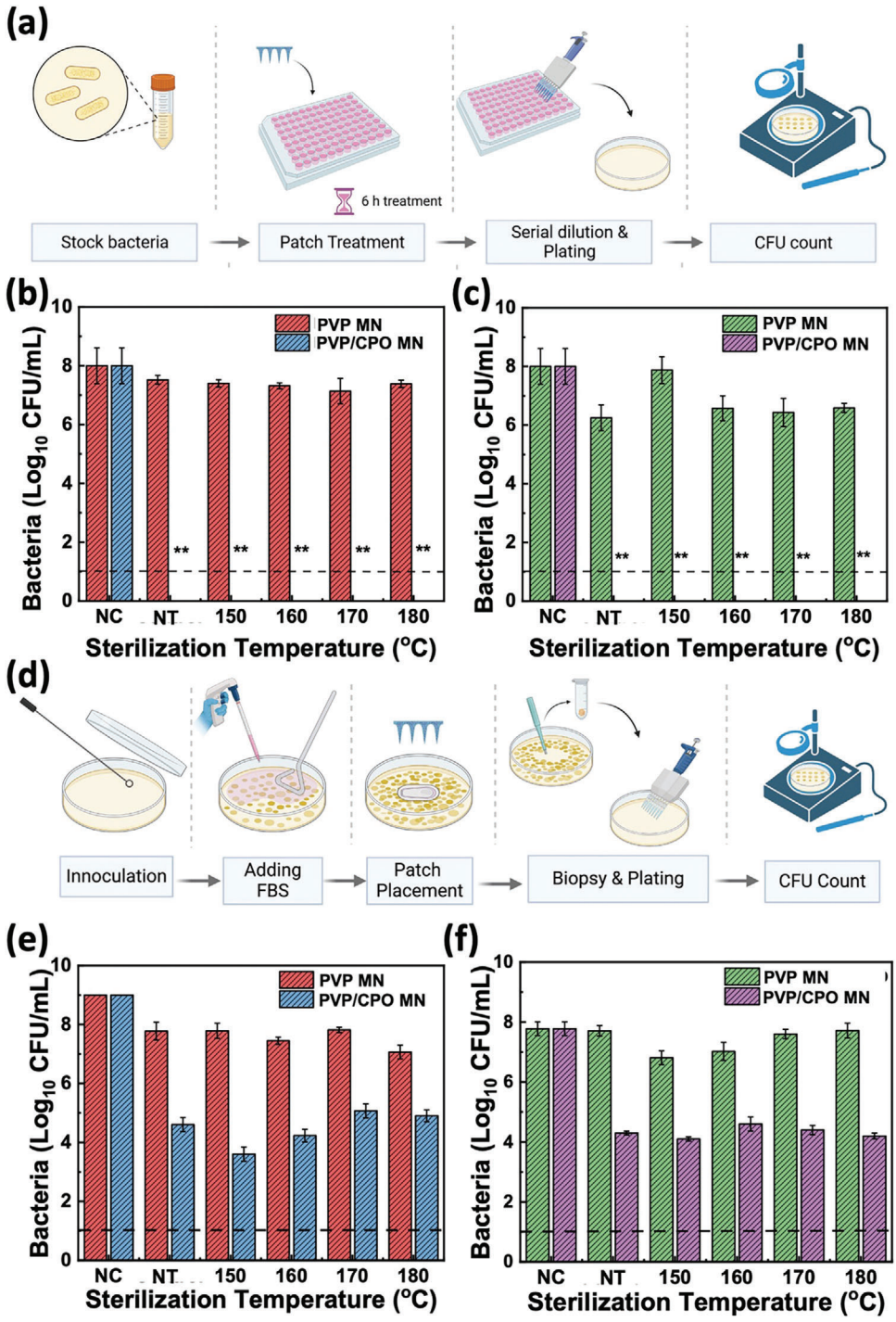

Figure 3. Antibacterial properties of PVP/CPO MN at different sterilization temperatures. a) Schematic illustration of the procedure for assessing the antibacterial properties of PVP/CPO MNs against planktonic bacteria. b) Results of the antibacterial assay against planktonic *P. aeruginosa* and c) *S. aureus*. d) Schematic illustration of the procedure for assessing the antibacterial properties of PVP/CPO MNs against biofilm models of P. aeruginosa and e) *S. aureus*. (NC refers to negative control without treatment, and NT refers to PVP/CPO MNs without heat sterilization treatment).

significantly deter the overall antibacterial performance of the MN structures toward a biofilm model. Based on these previous observations, the MN sterilized at 150 °C was selected for further experimentation due to the optimal mechanical properties with slightly pronounced antibacterial efficacy compared to other samples. Next, to evaluate the minimum number of treatments required to completely eradicate a biofilm infection, MN patches were applied repeatedly at the same treatment region and monitored the kill-off over time (**Figure** 4a). In Figure 4b, a decreasing trend in the *P. aeruginosa* population was observed, with

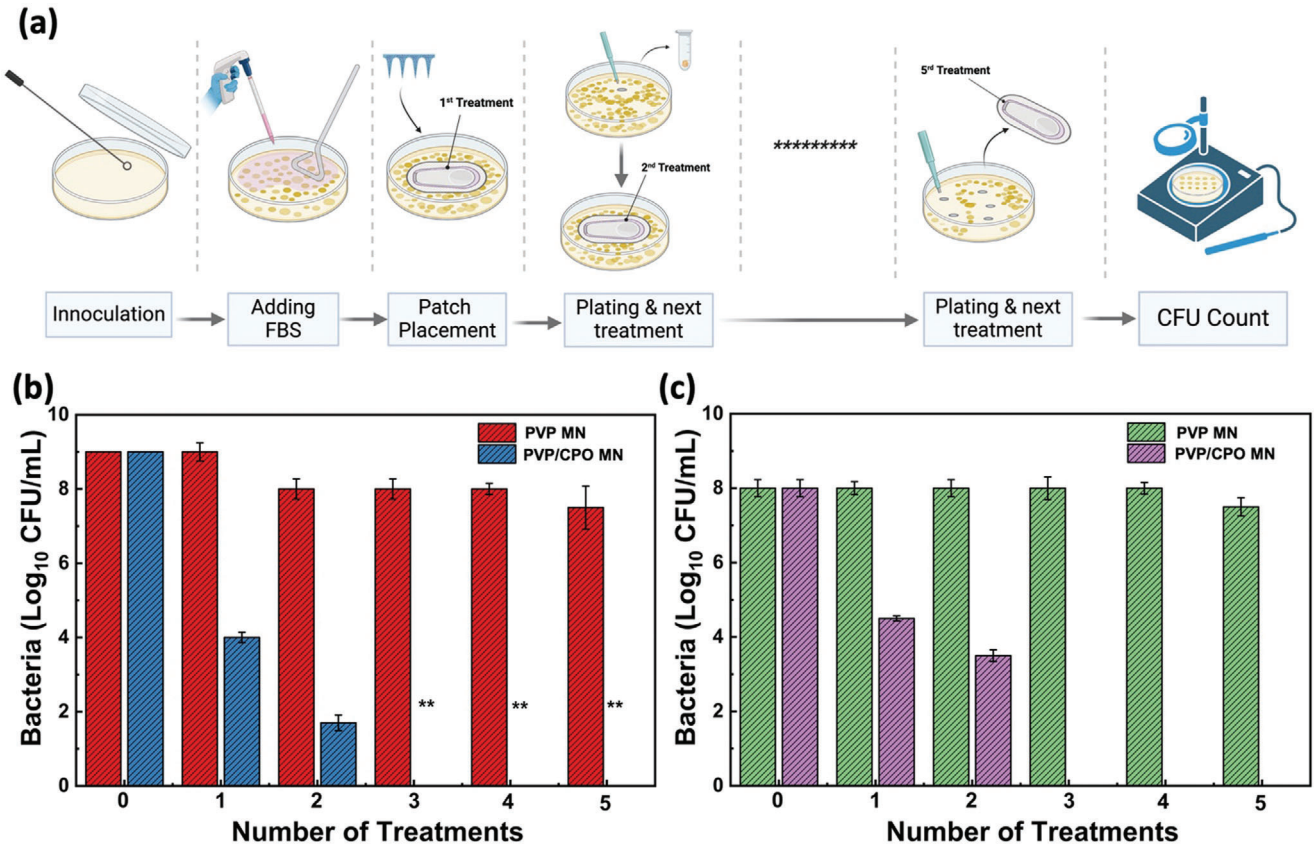

Figure 4. Repeated application of MNs on biofilm infections. a) Schematic illustration of multiple applications of PVP/CPO MNs with optimized heat sterilization process at 150 °C and assessment of bacterial eradication effect after different treatments, along with the corresponding results for b) *P. aeruginosa* and (c) *S. aureus* biofilm.

complete eradication of biofilm (undetectable) after three rounds of PVP/CPO treatment. Similarly, the *S. aureus* biofilm model also showed a complete kill-off of the bacterial populations after 3 treatment cycles. Thus, it was concluded that a minimum of 3 rounds of MN treatment is required to completely eradicate the bacterial population even in a non-clinical in vitro testing scenario.

3.3. In Vitro Biocompatibility Assessment

In vitro, biocompatibility assessment of the optimized MN structures upon application on the wound surface was analyzed using HCT-8 epithelial cells. The proliferation and viability of the cells were assessed by monitoring colorimetric OD measurements using the WST-8 assay over a period of 3 days (**Figure 5a**). As observed from Figure 5b, the cell proliferation in the control wells exhibited a gradual increase from 0.25 to 0.82 over the course of three days. On the contrary, PVP MN showed increased cell proliferation compared to control samples which was probably due to the polymer acting as a scaffold for HCT-8 cells to form multilayers. Interestingly. The PVP/CPO MN observed a clear increase in cell proliferation of ≈1.5 after 3 days of repeated exposure. Increased cell proliferation suggests the decomposition of CPO resulted in elevated oxygen levels in the PVP/CPO wells, leading to increased energy production and potentially faster cell proliferation. A similar increase in cell proliferation with the decomposition of CPO was observed by Mollajavadi et al.[66] Further, to complement these observations from the WST-8 assay a trypan and live-dead staining was employed to visualize cell viability and cell membrane integrity. The live-dead staining images showed a pronounced green-to-red ratio for the PVP/CPO MN structures after 3 cycles of exposure, similar to the control and PVP treatment groups, confirming enhanced biocompatibility (Figure 5c). Further, a simple trypan blue staining test was performed to visualize the increased cell proliferation of the cells upon MN treatment. As observed from Figure 5d, the PVP and PVP/CPO MN structures showed a clear multilayer formation from treatment day 1 to day 3, while the control remained comparable to day 1. A positive control sample, treated with 1% Triton-X solution to induce complete cell death, served as the reference for comparing the obtained cell proliferation images. Both PVP and PVP/CPO samples demonstrated heightened cell viability compared to the control, distinct from the complete kill-off observed in the positive control. These results collectively validate the materials utilized in the study, affirming the biocompatibility of the manufacturing process, and indicating its suitability for application in an infected wound environment.

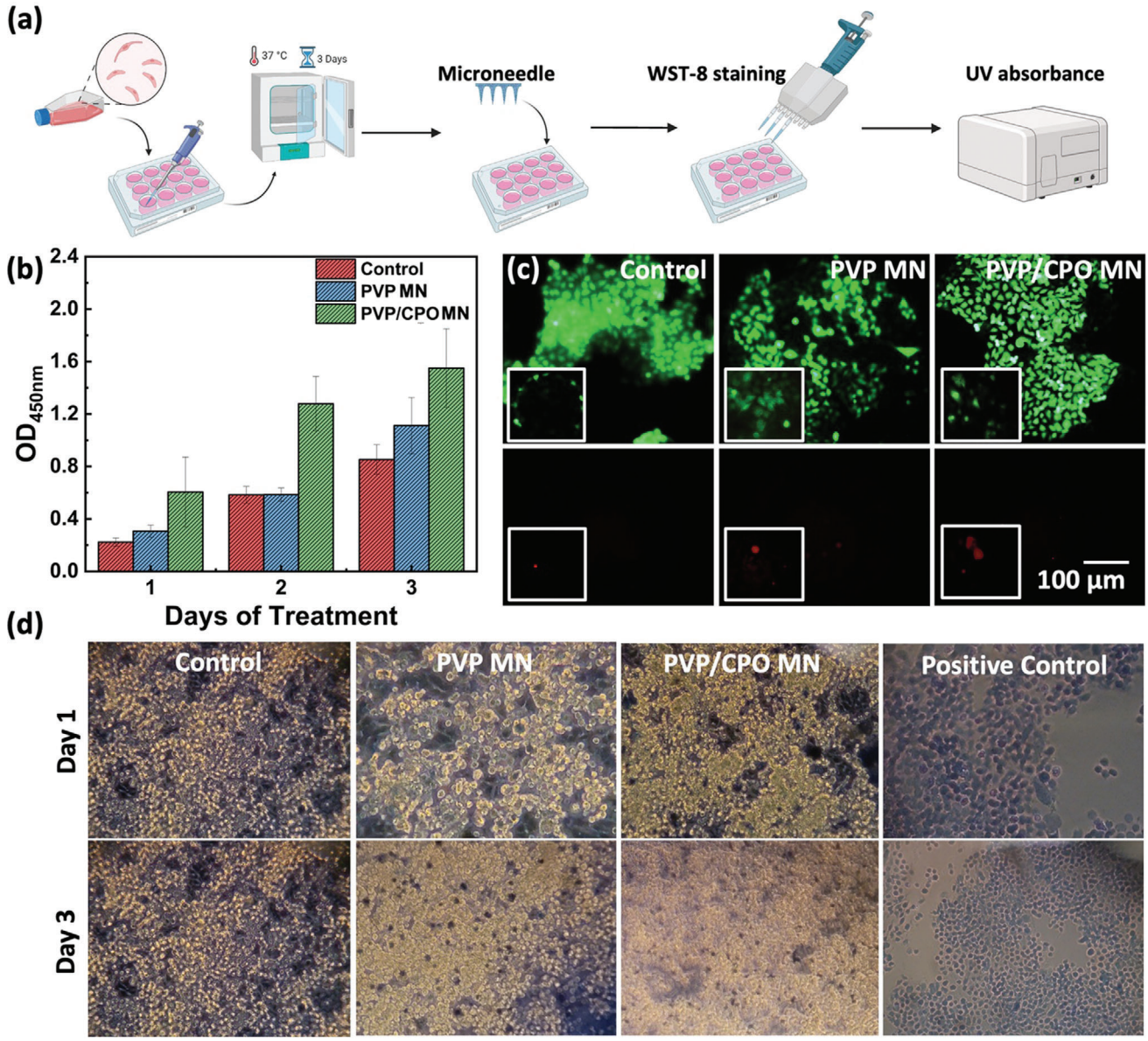

Figure 5. Biocompatibility assessment of the PVP/CPO microneedles sterilized at 150 °C. a) Illustration depicting the process for biocompatibility assessment. b) WST-8 cell proliferation assay. c) Live (green) and dead (red) fluorescence staining images after 3 days of exposure to different conditions. d) Trypan blue staining images after 1 day and 3 days of exposure to different conditions.

3.4. In Vitro Pathogenesis Inactivation

Subsequently, it was necessary to test the ability of MNs to inhibit bacterial pathogenesis, including adhesion, intracellular invasion, and intercellular translocation (Figure S5 Supporting Information). A bacterially infected in vitro wound model was created to evaluate the effect of the MN treatment in inhibiting adhesion, invasion (**Figure 6**a), and translocation (Figure 6b) characteristics using Caco-2 epithelial cells. As shown in Figure 6c, PVP MN showed a marginal reduction in the adhesion, invasion, and translocation characteristics (<35%) in the bacterial population compared to the control samples toward *P. aeruginosa* infection. On the other hand, with PVP/CPO MN treatment, a remarkable 90–95% decrease in all three bacterial pathogenesis was observed. Similarly, in an *S. aureus* infection model, the PVP treatment group showed no significant bacterial reduction (<25%) compared to the control. However, with PVP/CPO treatment, enhanced inhibition of the bacterial population (92–100%) was observed toward a *S. aureus* infection (Figure 6d). Interestingly, *S. aureus* demonstrated complete eradication (undetectable) of the intracellular bacterial population compared to that of the *P. aeruginosa* infection. This difference might be attributed to the enteroinvasive nature of *P. aeruginosa*, which resulted in a mild reduction in the intracellular effectiveness of the MN treatment.[67] These results validate the inhibitory effect of the MN treatment deterring the adhesion, invasion, and translocation pathogenesis

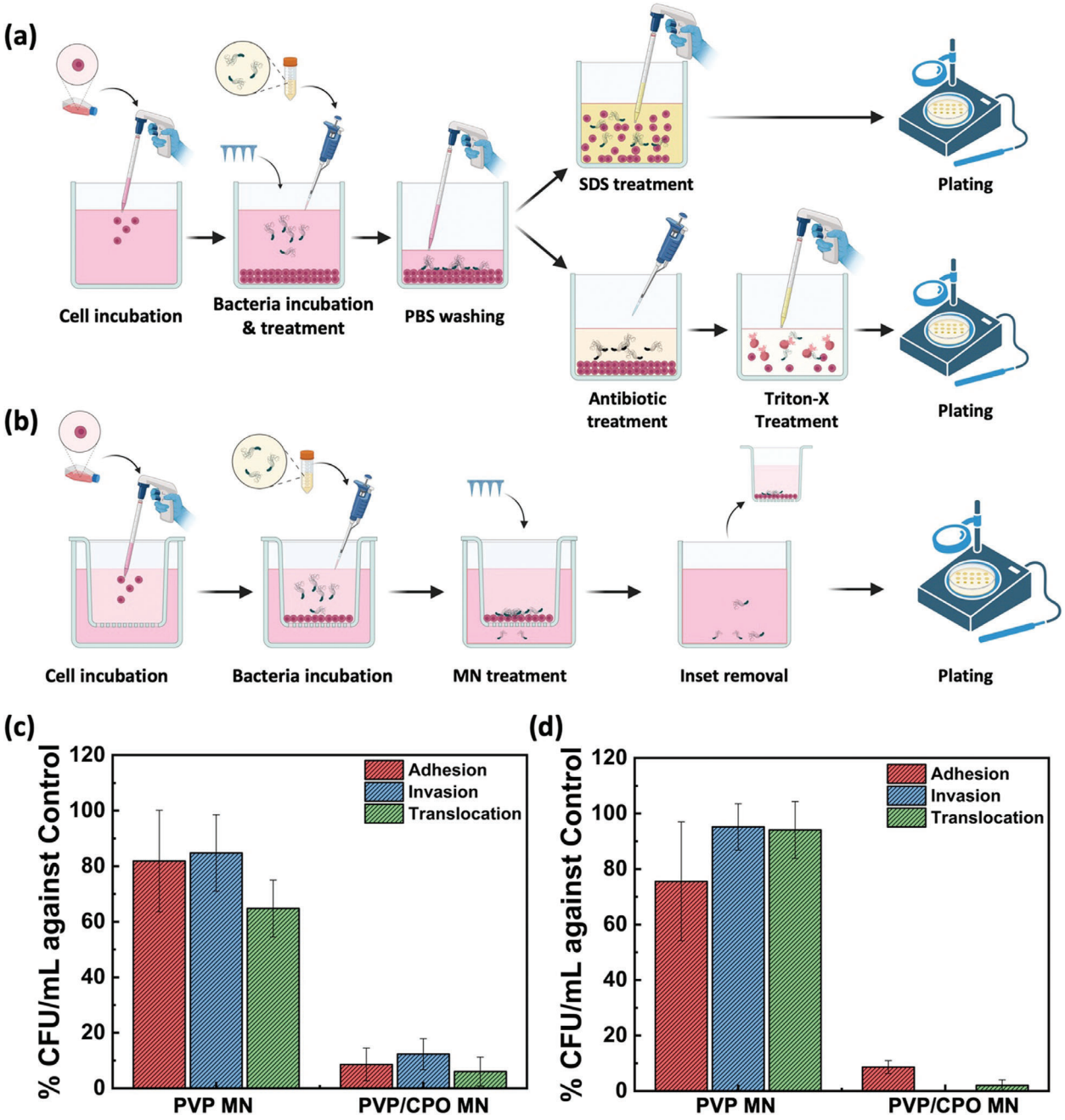

Figure 6. Host-pathogen analysis. a) Schematic illustration of the process for analyzing the effect of the MNs on the pathogens' adhesion and invasion (intracellularly invaded). b) Schematic representation of intercellular translocation (intercellular transmigrated) in the host cells. c) Bactericidal results of model infections with *P. aeruginosa* and d) *S. aureus*.

of the bacterium which would be critical for a deep tissue infection model treatment.

3.5. In Vivo Wound Infection Assessment

Finally, an in vivo study was conducted using a porcine model to assess the effectiveness of PVP/CPO MN in bacterial eradication and wound healing against *P. aeruginosa* and *S. aureus* infections as shown in Figure S6 (Supporting Information). The complete timeline of the in vivo study, from wounding to treatment and euthanasia of the animals, is depicted in **Figure** 7a. Initially, all 12 wound beds across the 3 pigs exhibited an average bacterial count of ≈5.6-log CFU after 24 h of *P. aeruginosa* infection (Figure 7b). Progressively, over the treatment week, the control sterile gauze groups showed no observable change in the *P. aeruginosa* bacterial populations. Similarly to that of the control groups, PVP MN also showed no signs of reduction in the

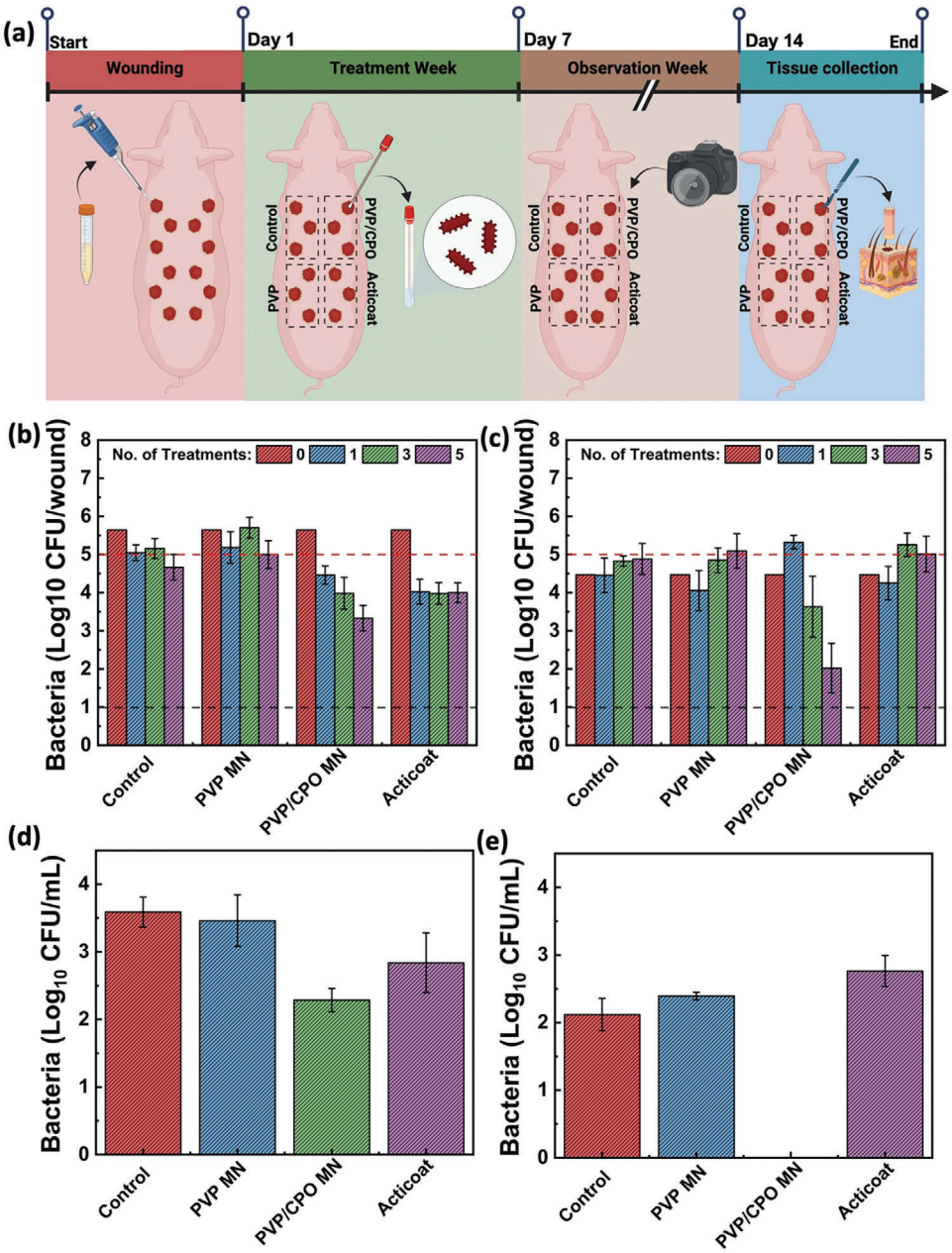

Figure 7. In vivo bactericidal assessment of the treatment. a) Experimental timeline of the MN treatment. Viable bacteria collected from swabs of superficial wound exudate infected with b) *P. aeruginosa* and c) *S. aureus* at different time points of treatment. The viable intracellularly invaded bacteria d) *P. aeruginosa* and e) *S. aureus* in the wound tissue at the end of the study with different treatments.

bacterial CFU counts. On the contrary, Acticoat dressing exhibited a significant reduction in the bacterial population after one treatment cycle, with marginal reduction observed thereafter. This can be attributed to the limited efficacy of the Acticoat surface in delivering antimicrobials (silver) to the bacterial population encased within a biofilm structure on a wound surface. However, upon exposure to PVP/CPO MN, a distinct reduction profile was observed, with a minimum of 0.5-log CFU reduction per treatment cycle against *P. aeruginosa* infection. Similarly, in the *S. aureus* infection model, no significant reduction in the bacterial population was observed in both the control and the PVP MN wound groups after 5 rounds of treatment, consistent with previous observations. Interestingly, the Acticoat treatment group showed no noticeable reduction in the *S. aureus* population, in contrast to the observed reduction in the *P. aeruginosa* infection. The decrease in therapeutic efficacy of Acticoat can be explained by the structural variances between Gram-positive and Gram-negative bacteria, particularly the peptidoglycan layer. Similar results of inability of Acticoat to not inhibit the *S. aureus* populations were observed by Ravensdale et al.[68,69] Nevertheless, with PVP/CPO MN treatment, a clear reduction in the bacterial population from 4.4-log CFU to 1.8-log CFU was observed after

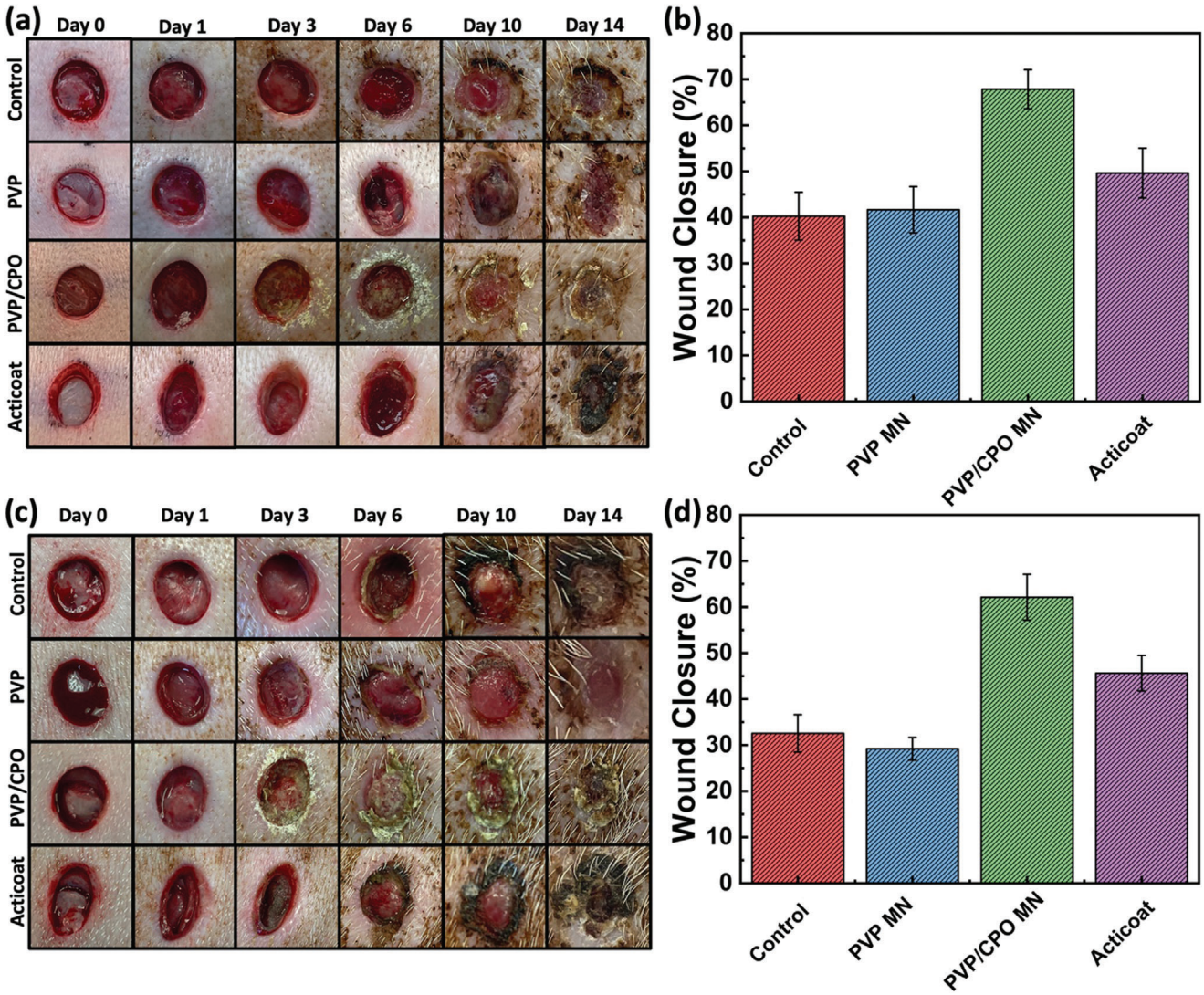

Figure 8. In vivo wound healing rate assessment. Images of the pig's infected dermal wounds with a) *P. aeruginosa* and c) *S. aureus* during the treatment phase (days 1–6) and observation phase (days 7–14). Final wound closure percentage with different treatments at the end of the study for wounds infected with b) *P. aeruginosa* and d) *S. aureus*.

5 days of treatment. Thus, the developed PVP/CPO MN treatment showed a clear reduction of at least 2-log CFU (99% reduction) irrespective type of the bacterial population which is often considered a meaningful reduction indicative of treatment success.[70] After terminating the in vivo study, resected segments of the wound bed were plated to evaluate the altercation in intracellularly invaded pathogens counts in response to the treatment groups (Figure S7, Supporting Information). As expected, both the control and PVP MN treatments demonstrated comparable invasion counts (≈3.5-log CFU) toward *P. aeruginosa* bacterial infection as shown in Figure 7d. Similarly, the Acticoat treatment group showed a comparable intracellular bacterial population to that of the control wound groups. However, the application of PVP/CPO MN resulted in a notable reduction of 1.2-log CFU compared to a control group in *P. aeruginosa* infection. On the other hand, similar bacterial populations ranging from 2 to 2.6-log CFU were observed in the control, PVP, and Acticoat treatment groups in an *S. aureus* wound infection (Figure 7e). Remarkably, complete eradication (undetectable) of the bacterial population was achieved with PVP/CPO MN administration on the *S. aureus* infected wound surface. These results unequivocally underscore the superior efficacy of PVP/CPO treatment in reducing bacterial loads on the wound surface, surpassing the performance of standard-of-care silver dressing.

Finally, visual photographic images of the infected wound bed before and after the onset of infection and treatments were recorded over the course of the experimental timeline to evaluate the level of wound closure. Images were captured at key time points: on the day of wound and infection induction (day 0), 24 h after wound infection and starting the treatments (day 1), during the treatment phase (day 3 and 6), and post-treatment phase (day 10 and 14). It is evident from **Figure** 8a that the control group observed a gradual reduction in redness and tissue development from day 1 to day 14, while its scar redness resulted from

the processes of normal wound healing toward *P. aeruginosa* infection.[69] Additionally, the PVP MN treatment group similarly exhibited wound progression, with persistent unhealed wounds evident on day 14. On the other hand, the Acticoat treatment groups exhibited clear signs of scab formation, indicative of mild toxicity with epithelizing and proliferating wounds. These observations are supported by Fong et al.[71] cautioning the application of Acticoat on epithelializing and proliferating wounds. However, as expected, the wound area of the PVP/CPO MN treatment was observed to decrease more rapidly with no signs of visual redness on 14 days of experimentation. This observation was further validated by calculating the wound area of each treatment group with *P. aeruginosa* infection and comparing it against the wound area from day 1 (Figure 8b). The % closure of wounds exposed to PVP/CPO MN treatment groups demonstrated a faster healing rate of ≈28% compared to other treatment groups in response to *P. aeruginosa* infection. Similarly, wounds infected with the *S. aureus* bacterium also exhibited deeper and milder redness compared to wounds exposed to the control and PVP MN treatment groups after 14 days of wound creation as shown in Figure 8c. Additionally, the Acticoat treatment group showed similar scab formation, consistent with observations from the *P. aeruginosa* infection. Consequently, the PVP/CPO MN treatment group observed a clear reduction in wound area, with at least a 30% faster healing rate compared to the control samples (Figure 8d). These results collectively highlight the effectiveness of the developed PVP/CPO MN technology to inhibit bacterial pathogens both topically and intracellularly in an in vivo bacterially infected wound environment. A summary of various MN-based technologies for effectively eradicating bacterially infected wounds, as reported in the literature, is tabulated, and compared in Table S1 (Supporting Information). As observed, this is the first study to validate the effectiveness of MNs in eradicating intercellular and intracellular pathogens and thereby promoting the wound healing process in an in vivo porcine model. Additionally, this work investigates the scalable and rapid production of these MNs, along with an effective sterilization procedure that does not compromise their functionality. These observations collectively suggest promising clinical and commercialization potential for this MN technology in managing infections and promoting healing in bacterially infected chronic wounds.

4. Conclusion

In summary, this work presents a systematic study investigating the scalable fabrication and heat sterilization of calcium peroxide-infused water-dissolvable microneedle structures aiming to effectively treat bacterial wound infections. In vitro, analysis demonstrated enhanced antibacterial properties toward planktonic and biofilm models and promoted biocompatible characteristics of the microneedle structures. Additionally, the developed microneedle technology was observed to clearly deter the adhesion, invasion, and translocation pathogenesis of the bacterium which would be critical for a deep tissue infection model treatment. Subsequently, the in vivo analysis revealed substantial reductions in both extracellular and intracellular bacterial populations and accelerated wound healing and tissue regeneration compared to controls and standard care methods. These findings emphasize the potential of the microneedle patch technology for treating bacterially infected wounds, reducing the need for antibiotics and complicated surgical interventions. Moreover, given its promising potential, future efforts will focus on exploring the treatment efficacy across diverse in vivo chronic wound models, aiming to enhance the understanding of microneedle treatment before advancing to clinical trials.

Supporting Information

Supporting Information is available from the Wiley Online Library or from the author.

Acknowledgements

The authors thank the staff of Birck Nanotechnology Center and the School of Material Engineering at Purdue University for their support. Funding for this project was provided by the Purdue Research Foundation Proof of Concept award and R. R. Startup funds at Purdue University. The authors also acknowledge the partial support from the National Institutes of Health (IR21DK128715-01A1) and the National Institute of Food and Agriculture (13699514).

Conflict of Interest

The authors declare no conflict of interest.

Author Contributions

A.K. performed conceptualization, data curation, methodology, investigation, and formal analysis, and Wrote original draft; N.L.F.G. performed conceptualization, data curation, methodology, and investigation; D.S. performed software, investigation and acquired resources; R.M., C.C., and M.T. performed investigation and acquired resources; M.M. and. A.D.C. performed methodology and acquired resources; A.K.B. and M.S performed methodology and did supervision; R.R. performed conceptualization, methodology, data curation, acquired funding, did supervision, project administration, and Wrote original draft.

Data Availability Statement

The data that support the findings of this study are available from the corresponding author upon reasonable request.

Keywords

biofilm infection, calcium peroxide, chronic wound, intracellular invasion, microneedle therapy

Received: February 8, 2024
Revised: April 20, 2024
Published online: May 25, 2024

[1] C. K. Sen, *Adv Wound Care* **2021**, *10*, 281.
[2] C. K. Sen, *Adv Wound Care* **2023**, *12*, 657.
[3] C. K. Sen, *Adv Wound Care* **2019**, *8*, 39.
[4] J. Bao, L. Zhou, G. Liu, J. Tang, X. Lu, C. Cheng, Y. Jin, J. Bai, *Biosci Trends* **2022**, *16*, 107.

[5] V. Atella, A. Piano Mortari, J. Kopinska, F. Belotti, F. Lapi, C. Cricelli, L. Fontana, *Aging Cell* **2019**, *18*, 12861.
[6] G. Han, R. Ceilley, *Adv. Ther.* **2017**, *34*, 599.
[7] D. Stephanie, C. Allie, F. Haley, E. Jake, A. R. Horswill, K. P. Rumbaugh, *Infect. Immun.* **2014**, *82*, 4718.
[8] C. Attinger, R. Wolcott, *Adv Wound Care* **2012**, *1*, 127.
[9] A. G. Goswami, S. Basu, T. Banerjee, V. K. Shukla, *Eur J Med Res* **2023**, *28*, 157.
[10] J. Khan, S. M. Tarar, I. Gul, U. Nawaz, M. Arshad, *3 Biotech* **2021**, *11*, 169.
[11] C. K. Sen, S. Roy, S. S. Mathew-Steiner, G. M. Gordillo, *Plast. Reconstr. Surg.* **2021**, *148*, 148e1.
[12] M. J. Worley, *Immune Evasion and Persistence in Enteric Bacterial Pathogens*, *15*, Taylor and Francis Ltd, Oxfordshire United Kingdom **2023**.
[13] K. Zegadło, M. Gieroń, P. Żarnowiec, K. Durlik-Popińska, B. Kręcisz, W. Kaca, G. Czerwonka, *Int. J. Mol. Sci.* **2023**, *24*, 1707.
[14] R. Schülein, A. Seubert, C. Gille, C. Lanz, Y. Hansmann, Y. Piémont, C. Dehio, *J. Exp. Med.* **2001**, *193*, 1077.
[15] T. Maheswary, A. A. Nurul, M. B. Fauzi, *Pharmaceutics* **2021**, *13*, 981.
[16] C. E. Di Russo, S. J. E, *Microbiol. Spectr.* **2016**, *4*, 1.
[17] A. Thakur, H. Mikkelsen, G. Jungersen, *J Immunol Res* **2019**, *2019*, 1356540.
[18] L. K. Vestby, T. Grønseth, R. Simm, L. L. Nesse, *Antibiotics* **2020**, *9*, 59.
[19] M. G. Mathipa, A. K. Bhunia, M. S. Thantsha, *PLoS One* **2019**, *14*, 0220321.
[20] M. R. Chaaban, A. Kejner, S. M. Rowe, B. A. Woodworth, *Am J Rhinol Allergy* **2013**, *27*, 387.
[21] S. Nejati, D. Sarnaik, S. Gopalakrishnan, V. Kasi, A. Krishnakumar, S. Hyde, R. McCain, K. Park, J. S. Johnson, R. Rahimi, *Adv. Mater. Technol.* **2024**, *9*, 2300810.
[22] S. Gopalakrishnan, R. Thomas, S. Sedaghat, A. Krishnakumar, S. Khan, T. Meyer, H. Ajieren, S. Nejati, J. Wang, M. S. Verma, P. Irazoqui, R. Rahimi, *Biosens Bioelectron X* **2023**, *14*, 100380.
[23] S. Kadian, S. Gopalakrishnan, V. Selvamani, S. Khan, T. Meyer, R. Thomas, M. M. Rana, P. P. Irazoqui, M. Verma, R. Rahimi, *IEEE Trans. Biomed. Eng.* **2023**, *71*, 1565.
[24] Y. J. Cheah, M. R. Buyong, M. H. Mohd Yunus, *Polymers* **2021**, *13*, 3790.
[25] L. Tewarie, N. Chernigov, A. Goetzenich, A. Moza, R. Autschbach, R. Zayat, *Annals Thorac. Cardiovasc. Surg.* **2018**, *24*, 139.
[26] H. X. Nguyen, C. N. Nguyen, *Pharmaceutics* **2023**, *15*, 277.
[27] A. Krishnakumar, G. K. Mani, R. R. Suresh, A. J. Kulandaisamy, K. Tsuchiya, J. Bosco, B. Rayappan, *Nanosensors for Futuristic Smart and Intelligent Healthcare Systems*, CRC Press, Boca Raton, Florida **2015**.
[28] M. Ochoa, R. Rahimi, B. Ziaie, *IEEE Rev Biomed Eng* **2014**, *7*, 73.
[29] J. Nandhini, E. Karthikeyan, S. Rajeshkumar, *Boca Raton, Florida* **2024**, *6*, 26.
[30] A. Varma, A. Warghane, N. K. Dhiman, N. Paserkar, V. Upadhye, A. Modi, R. Saini, *Front Cell Infect Microbiol* **2023**, *13*.
[31] S. Darvishi, S. Tavakoli, M. Kharaziha, H. H. Girault, C. F. Kaminski, I. Mela, *Angew. Chem., Int. Ed.* **2022**, *61*, 202112218.
[32] N. Kamaly, B. Yameen, J. Wu, O. C. Farokhzad, *Chem. Rev.* **2016**, *116*, 2602.
[33] S.-J. Yang, J.-O. Jeong, Y.-M. Lim, J.-S. Park, *Mater. Des.* **2021**, *201*, 109485.
[34] J. Ziesmer, P. Tajpara, N.-J. Hempel, M. Ehrström, K. Melican, L. Eidsmo, G. A. Sotiriou, *Adv. Mater. Technol.* **2021**, *6*, 2001307.
[35] S. Abdelghany, W. Alshaer, Y. Al Thaher, M. Al Fawares, A. G. Al-Bakri, S. Zuriekat, R. S. Mansour, *Beilstein J. Nanotechnol.* **2022**, *13*, 517.
[36] Y. Liang, Y. Liang, H. Zhang, B. Guo, *Asian J Pharm. Sci.* **2022**, *17*, 353.
[37] D. Chinemerem Nwobodo, M. C. Ugwu, C. Oliseloke Anie, M. T. S. Al-Ouqaili, J. Chinedu Ikem, U. Victor Chigozie, M. Saki, *J Clin Lab Anal* **2022**, *36*, 24655.
[38] A. Zareei, V. Kasi, A. Thornton, U. H. Rivera, M. Sawale, M. K. Maruthamuthu, Z. He, J. Nguyen, H. Wang, D. K. Mishra, R. Rahimi, *Nanoscale* **2023**, *15*, 11209.
[39] V. Selvamani, A. Zareei, A. Elkashif, M. K. Maruthamuthu, S. Chittiboyina, D. Delisi, Z. Li, L. Cai, V. G. Pol, M. N. Seleem, R. Rahimi, *Adv. Mater. Interfaces* **2020**, *7*, 1901890.
[40] J. M. V. Makabenta, A. Nabawy, C.-H. Li, S. Schmidt-Malan, R. Patel, V. M. Rotello, *Nat. Rev. Microbiol.* **2021**, *19*, 23.
[41] J. Kang, M. J. Dietz, K. Hughes, M. Xing, B. Li, *J. Antimicrob. Chemother.* **2019**, *74*, 1578.
[42] H. Li, X. Zhou, Y. Huang, B. Liao, L. Cheng, B. Ren, *Front. Microbiol.* **2021**, *11*.
[43] A. Roth, A. Krishnakumar, R. R. McCain, M. K. Maruthamuthu, M. McIntosh, Y. X. Chen, A. D. Cox, A. S. Hopf Jannasch, J. Nguyen, M. N. Seleem, R. Rahimi, *ACS Biomater. Sci. Eng.* **2023**, *9*, 3606.
[44] S. Chittiboyina, R. Rahimi, F. Atrian, M. Ochoa, B. Ziaie, S. A. Lelièvre, *ACS Biomater. Sci. Eng.* **2018**, *4*, 432.
[45] I. Woodhouse, S. Nejati, V. Selvamani, H. Jiang, S. Chittiboyina, J. Grant, Z. Mutlu, J. Waimin, N. S. Abutaleb, M. N. Seleem, R. Rahimi, *ACS Appl Bio Mater* **2021**, *4*, 5405.
[46] A. Roth, M. K. Maruthamuthu, S. Nejati, A. Krishnakumar, V. Selvamani, S. Sedaghat, J. Nguyen, M. N. Seleem, R. Rahimi, *Sci. Rep.* **2022**, *12*, 13927.
[47] J. Chen, H. Ma, H. Luo, H. Peng, Q. Yan, S. Pu, *J. Hazard. Mater.* **2024**, *464*, 132902.
[48] L. Karner, S. Drechsler, M. Metzger, P. Slezak, J. Zipperle, G. Pinar, K. Sterflinger, F. Leisch, J. Grillari, M. Osuchowski, P. Dungel, *Sci. Rep.* **2020**, *10*, 11494.
[49] R. K. Tweten, *Infect. Immun.* **2005**, *73*, 6199.
[50] N. Möller, S. Ziesemer, P. Hildebrandt, N. Assenheimer, U. Völker, J.-P. Hildebrandt, *PLoS One* **2020**, *15*, 0233854.
[51] A. Daddaoua, C. Molina-Santiago, J. de la Torre, T. Krell, J.-L. Ramos, *Nucleic Acids Res.* **2014**, *42*, 7654.
[52] V. C. Culotta, M. Yang, T. V O'Halloran, *Biochim. Biophys. Acta* **2006**, *1763*, 747.
[53] A. Ambrosch, S. Haefner, E. Jude, R. Lobmann, *Int. Wound J.* **2011**, *8*, 567.
[54] V. Selvamani, S. Kadian, D. A. Detwiler, A. Zareei, I. Woodhouse, Z. Qi, S. Peana, A. M. Alcaraz, H. Wang, R. Rahimi, *Langmuir* **2022**, *38*, 4014.
[55] T. Coenye, M. Bové, T. Bjarnsholt, *NPJ Biofilms Microbiomes* **2022**, *8*, 82.
[56] P. Ngamwongsatit, P. P. Banada, W. Panbangred, A. K. Bhunia, *J Microbiol Methods* **2008**, *73*, 211.
[57] A. Krishnakumar, S. Kadian, U. Heredia Rivera, S. Chittiboyina, S. A. Lelièvre, R. Rahimi, *ACS Biomater. Sci. Eng.* **2023**, *9*, 1620.
[58] H. Jiang, N. M. Carter, A. Zareei, S. Nejati, J. F. Waimin, S. Chittiboyina, E. E. Niedert, T. Soleimani, S. A. Lelièvre, C. J. Goergen, R. Rahimi, *ACS Appl Bio Mater* **2020**, *3*, 4012.
[59] V. Kasi, S. Sedaghat, A. M. Alcaraz, M. K. Maruthamuthu, U. Heredia-Rivera, S. Nejati, J. Nguyen, R. Rahimi, *ACS Appl. Mater. Interfaces* **2022**, *14*, 9697.
[60] R. Rahimi, U. Brener, S. Chittiboyina, T. Soleimani, D. A. Detwiler, S. A. Lelièvre, B. Ziaie, *Sens. Actuators, B* **2018**, *267*, 198.
[61] A. N. Antoniou, S. J. Powis, *Immunology* **2008**, *124*, 1.
[62] T. Waghule, G. Singhvi, S. K. Dubey, M. M. Pandey, G. Gupta, M. Singh, K. Dua, *Biomed. Pharmacother.* **2019**, *109*, 1249.
[63] S. P. Davis, B. J. Landis, Z. H. Adams, M. G. Allen, M. R. Prausnitz, *J. Biomech.* **2004**, *37*, 1155.
[64] Y. Deng, C. Yang, Y. Zhu, W. Liu, H. Li, L. Wang, W. Chen, Z. Wang, L. Wang, *Nano Lett.* **2022**, *22*, 2702.

[65] S. A. Ranamukhaarachchi, T. Schneider, S. Lehnert, L. Sprenger, J. R. Campbell, I. Mansoor, J. C. Y. Lai, K. Rai, J. Dutz, U. O. Häfeli, B. Stoeber, *Macromol. Mater. Eng.* **2016**, *301*, 306.
[66] M. Y. Mollajavadi, M. Saadatmand, F. Ghobadi, *Iran. Polym. J.* **2023**, *32*, 599.
[67] S. P. Diggle, M. Whiteley, *Microbiology* **2020**, *166*, 30.
[68] J. P. Barrett, E. Raby, F. Wood, R. Coorey, J. P. Ramsay, G. A. Dykes, J. T. Ravensdale, *Burns* **2022**, *48*, 941.
[69] J. Ravensdale, F. Wood, F. O'Brien, K. Gregg, *J Med Microbiol* **2016**, *65*, 397.
[70] C. Goodburn, C. A. Wallace, *Food Control* **2013**, *32*, 418.
[71] J. Fong, F. Wood, *Int. J. Nanomed.* **2006**, *1*, 441.